Journal of Solid State Chemistry 181 (2008) 3337–3343

Contents lists available at ScienceDirect

Journal of Solid State Chemistry

journal homepage: www.elsevier.com/locate/jssc

Synthesis, crystal structure, and property of one- and two-dimensional complexes based on paradodecatungstate-B cluster

Bao Li, Lihua Bi, Wen Li, Lixin Wu *

State Key Laboratory of Supramolecular Structure and Materials, College of Chemistry, Jilin University, Changchun 130012, PR China

ARTICLE INFO

Article history:
Received 21 May 2008
Received in revised form
26 August 2008
Accepted 1 September 2008
Available online 1 October 2008

Keywords:
Paradodecatungstate-B
Cadmium and copper ions
Crystal structure
Electrochemistry

ABSTRACT

Three polyoxotungstates, $Na_8[Cu(H_2O)_2(H_2W_{12}O_{42})]\cdot 30H_2O$ (**1**), $Na_8[Cd(H_2O)_2(H_2W_{12}O_{42})]\cdot 20H_2O$ (**2**), and $Na_{7.4}[Cd_{1.3}(H_2O)_2(H_2W_{12}O_{42})]\cdot 24H_2O$ (**3**), were synthesized and characterized by elemental and thermogravimetric (TG)analysis, infrared spectroscopy and X-ray single-crystal analysis. Both complexes **1** and **2** exhibit one-dimensional structure with two neighboring paradodecatungstate-B clusters, $[H_2W_{12}O_{42}]^{10-}$, linked by $[Cu(H_2O)_2]^{2+}$ or $[Cd(H_2O)_2]^{2+}$ units, while complex **3** displays a two-dimensional network structure. The electrochemical behaviors of complexes **1** and **3** were investigated in the buffer solution of pH 4.8. The results of electrocatalysis reveal that the reduced species of complexes **1** and **3** are electrocatalytically active for the reduction of nitrite. Complex **1** exhibits the electrocatalytic activity for the reduction of nitrate as well. The surface photovoltage spectroscopy (SPS) and electric field-induced SPS (EFISPS) measurements show that the surface photovoltage behavior of complex **1** is complicated while complex **3** bears the property of n-type semiconductor.

1. Introduction

Polyoxometalates (POMs) have been one of the remarkable and rich classes of inorganic clusters, which are usually constructed by early transition metals, especially tungsten, molybdenum and vanadium [1]. In the past several years, much attention has been paid on the design and synthesis of the complexes with novel crystal structure and functional properties, while most of which exist in discrete cluster state [2]. Due to the diverse potential applications in the interdisciplinary areas, especially in functional materials, extended POMs researches become more attractive based on a fundamental interest, such as linked or cross-linked POMs [3]. Generally, there are two types of polymeric POMs, one of which is that the clusters join with each other directly without the introduction of any other metals [4]. The other is that the clusters are connected by additional metal ions, especially those transition and lanthanide metal ions [5]. Comparing with the polymeric POMs without additional binding metal ions, the POMs networks with extra binding metal ions have been developed more widely due to the convenience and facility to connect discrete clusters. Such polymeric structures are surely important because of the multiformity of structure and function for these bonded clusters. To date, various metal-supporting POMs have been synthesized and characterized, such as $(NH_4)_2[Ni_4(1,2\text{-diaminopropane})_2(PW_9O_{34})_2]\cdot 9H_2O$ [6], $Co_2(4,4\text{-bipy})_6(W_6O_{19})_2$ [7], $[Cu_3(4,7\text{-phen})_3]_2Mo_{14}O_{45}$ [8], $[Zn_2(\text{terephthalate})(4,4\text{-bipy})\text{-}V_2O_6]$ [9] and $[Cu(enMe)_2]_7[V_{16}O_{38}(H_2O)]_2\cdot 4H_2O$ [10], which display rich and interesting structural and functional features. However, the design and synthesis of extended POMs are still a challenge and it is necessary to find an effective way by selecting an appropriate discrete cluster as basic unit for the construction of polymeric POMs. Considering coordination capability, we selected the paradodecatungstate-B cluster, $[H_2W_{12}O_{42}]^{10-}$, to be the primary building block. Several paradodecatungstate-B complexes with different counter ions have been synthesized and characterized [11–15]. This kind of anion is composed of four corner-sharing W_3O_{13} groups with two protons. Due to its stable structure and high reactive activity of the terminal oxygen atoms, paradodecatungstate-B cluster, as an ideal building block, has been also employed for the construction of extended metal bridged polyoxoanion, such as $H_2\{[K(H_2O)_2]_2[Ln(H_2O)_5]_2(H_2M_{12}O_{42})\}$ ($M=$ W, Mo), $[(Co(H_2O)_4)_2(H_2W_{12}O_{42})]_n^{6n-}$, and $[Cu(en)_2]_3[\{Cu(en)_2\}_2(H_2W_{12}O_{42})]\cdot 12H_2O$ [16–20].

To explore new structures based on paradodecatungstate-B clusters, we tried the reactions under controlled conditions and we really obtained some interesting complexes. In this paper, we described the synthesis, crystal structure, electrochemistry and photovoltage property of one copper (II) connected POM complex **1**, and two cadmium (II) connected POM complexes **2** and **3**. The frameworks of the complexes are supported by paradodecatungstate-B clusters. Because the structure of complex **2** is quite similar to the one that has been described in the literature [21],

* Corresponding author. Fax: +86 431 85193421.
E-mail address: wulx@jlu.edu.cn (L. Wu).

0022-4596/$ - see front matter © 2008 Elsevier Inc. All rights reserved.
doi:10.1016/j.jssc.2008.09.009

we mainly concentrate our description and discussion on complexes **1** and **3**.

2. Experimental

2.1. Materials and physical measurements

Doubly distilled water was used throughout the experiments. All reagents were commercially available and used without further purification. Buffer solution was prepared from 0.5 M NaAc and 0.5 M HAc. For the electrocatalysis experiments, the solutions of $NaNO_3$ and $NaNO_2$ were freshly prepared before use. All solutions were degassed with pure nitrogen gas for at least 30 min before use.

Elemental analysis (Na, Cu, Cd and W) were performed on a PLASMA-SPEC (I) inductively coupled plasma (ICP) spectrometer. FT-IR spectra were carried out on a Bruker Vertex 80 V FT-IR spectrometer equipped with a DTGS detector (32 scans) with a resolution of 4 cm^{-1} on KBr pellets. Thermogravimetric (TG) analyses were performed on a Perkin-Elmer TGA-7 instrument in flowing air with a heating rate of 10 °C min^{-1}. All electrochemical experiments were performed on a LK98BII electrochemical workstation at room temperature. A three-electrode electrochemical cell was used with a glassy carbon electrode (GCE) as the working electrode, a platinum wire as the counter and a Ag/AgCl electrode as the reference. The GCE was polished with 1.0, 0.3 and 0.05 μm α-Al_2O_3 powders successively, and sonicated in water for about 15 min after each polishing step. Finally, the electrode was washed with acetone and dried with a nitrogen stream immediately before use. Formal potentials (E_f) were estimated as average values of anodic (E_{pa}) and cathodic (E_{pc}) peak potentials, i.e., $E_f = (E_{pa}+E_{pc})/2$. The surface photovoltage (SPV) spectroscopic instrument was home-made and composed of xenon lamp of 500 W, precision monochromators, SRS-830 Lock-in amplifier, chopper and computer.

2.2. Synthesis

2.2.1. $Na_8[Cu(H_2O)_2(H_2W_{12}O_{42})]\cdot 30H_2O$ (**1**)

$Na_2WO_4\cdot 2H_2O$ (3.298 g, 10 mmol) and V_2O_5 (0.182 g, 1 mmol) were dissolved in 30 mL of water, and the pH of the mixture was adjusted to 4.8 by adding dilute HCl. The solution was then heated to 80 °C and kept at this temperature for 15 min. A clear solution was obtained, and to the solution was added $Cu(NO_3)_2\cdot 6H_2O$ (0.591 g, 2 mmol) subsequently. Diluted HCl was added again when turbidity occurs and the final pH was adjusted to 4.8. About 20 min later, the solution was cooled to room temperature and filtered. Slow evaporation of the filtrate generates light green block crystals. The yield was 60% (based on $Cu(NO_3)_2\cdot 6H_2O$). Anal. calc. (Found) (%) for $Na_8[Cu(H_2O)_2(H_2W_{12}O_{42})]\cdot 30H_2O$(**1**): Na 4.97 (5.09), W 59.56 (60.84), Cu 1.72 (1.78). IR (KBr pellet, cm^{-1}): 1630, 1579, 1417, 943, 875, 835, 806, 710, 501, 440.

2.2.2. $Na_8[Cd(H_2O)_2(H_2W_{12}O_{42})]\cdot 20H_2O$ (**2**)

Similar procedures were taken as mentioned above by using $CdCl_2\cdot 2.5H_2O$ (0.456 g, 2 mmol) instead of $Cu(NO_3)_2\cdot 6H_2O$. Colorless crystals were obtained in 2 weeks. The yield was 45% (based on $CdCl_2\cdot 2.5H_2O$). Anal. Calc. (Found) (%) for $Na_8[Cd(H_2O)_2(H_2W_{12}O_{42})]\cdot 20H_2O$ (**2**): Na 5.15 (5.26), W 61.75 (63.07), Cd 3.15 (3.26). IR (KBr pellet, cm^{-1}): 1635, 1576, 1415, 935, 887, 837, 798, 702, 499, 441.

2.2.3. $Na_{7.4}[Cd_{1.3}(H_2O)_2(H_2W_{12}O_{42})]\cdot 24H_2O$ (**3**)

$Na_2WO_4\cdot 2H_2O$ (3.298 g, 10 mmol) and V_2O_5 (0.182 g, 1 mmol) were added to 1 M of CH_3COONa/CH_3COOH buffer solution (pH 4.8), and the mixture was heated to 80 °C and then $CdCl_2\cdot 2.5H_2O$ (0.456 g, 2 mmol) was added. The mixture was stirred and heated for an hour at this temperature. During this period, the solution kept clear. After that, the solution was cooled to room temperature and filtered, the filtrate was kept in air and a colorless crystal was obtained in 2 weeks. The yield was 65% (based on $CdCl_2\cdot 2.5H_2O$). Anal. calc. (Found) (%) for $Na_{7.4}[Cd_{1.3}(H_2O)_2(H_2W_{12}O_{42})]\cdot 24H_2O$ (**3**): Na 4.64 (4.80), W 60.20 (61.71), Cd 3.99 (4.10). IR (KBr pellet, cm^{-1}): 1631, 1577, 1419, 945, 906, 875, 835, 804, 708, 501, 438.

2.2.4. Crystallographic data collection and refinement

A light green block single crystal of complex **1** ($0.052\times 0.056\times 0.062\ mm^3$) was set on the end of a glass capillary, and the data were collected on a Rigaku R-AXIS RAPID IP diffractometer with graphite monochromated Mo$K\alpha$ radiation ($\lambda = 0.71073$ Å) at 293 K in the range of $3.14^\circ<\theta<27.48^\circ$. Empirical absorption correction based on equivalent reflections was applied. A total of 31,023 (14,405 unique, $R_{int} = 0.0610$) reflections were measured ($-16\leqslant h\leqslant 16$, $-16\leqslant k\leqslant 17$, $-26\leqslant l\leqslant 26$). A colorless block single crystal of complex **2** ($0.085\times 0.096\times 0.101\ mm^3$) was fixed to the glass capillary, the data were obtained on the same diffractometer under the same condition of complex **1** in the range of $3.03^\circ<\theta<27.49^\circ$. Empirical absorption correction based on equivalent reflections was applied. A total of 13,593 (6235 unique, $R_{int} = 0.0524$) reflections were measured ($-14\leqslant h\leqslant 14$, $-15\leqslant k\leqslant 15$, $-15\leqslant l\leqslant 15$). Indexing and intensity data collection for **3** (colorless block, $0.035\times 0.036\times 0.039\ mm^3$) were also performed on the same diffractometer in the range of $3.04^\circ<\theta<27.50^\circ$ under the same condition as complex **1**. Empirical absorption correction based on equivalent reflections was applied. A total of 14,716 (6790 unique, $R_{int} = 0.0481$) reflections were measured ($-14\leqslant h\leqslant 14$, $-16\leqslant k\leqslant 16$, $-15\leqslant l\leqslant 16$).

The three complexes were all solved by direct method and refined by full-matrix least-squares fitting on F^2 using the SHELXTL-97 software. A summary of the crystallographic data and structural refinements for complexes **1**, **2** and **3** are listed in

Table 1
Crystal data and structure refinement of complexes **1**, **2** and **3**

Complex	**1**	**2**	**3**
Formula weight	3704.02	3572.74	3664.73
Temperature (K)	293(2)	293(2)	293(2)
λ (Å)	0.71073	0.71073	0.71073
Crystal system	Triclinic	Triclinic	Triclinic
Space group	*P*–1	*P*–1	*P*–1
a (Å)	13.081(4)	11.243(5)	10.973(4)
b (Å)	13.160(6)	11.961(5)	12.836(6)
c (Å)	20.127(6)	12.034(5)	13.014(5)
α (deg)	78.294(12)	64.510(17)	65.700(17)
β (deg)	78.524(11)	71.570(15)	67.410(14)
γ (deg)	72.593(11)	74.550(19)	69.150(18)
Volume (Å^3)	3201.7(17)	1369.7(10)	1499.2(10)
Z	2	1	1
d_{calcd} (g/cm^3)	3.907	4.332	4.059
Abs. coeff. (mm^{-1})	21.975	25.656	23.548
R_{int}	0.0610	0.0525	0.0482
F (0 0 0)	3450	1582	1630
GOOF on F^2	1.067	1.045	0.963
R [$I>2\sigma(I)$][a]	0.0429	0.0412	0.0470
R_w (all data)[b]	0.1160	0.0978	0.1212
$(Residues)_{max}$ (e/Å^3)	1.890	2.102	3.693
$(Residues)_{min}$ (e/Å^3)	−2.983	−4.493	−4.762

[a] $R = ||F_o|-|F_c||/|F_o|$.
[b] $R_w = [w(F_o^2-F_c^2)^2/w(F_o^2)^2]^{1/2}$.

Table 1. Selected bond lengths and angles with standard deviation in parentheses for complexes **1**–**3** are provided in Table 2.

3. Results and discussion

3.1. Synthesis

$Na_2WO_4 \cdot 2H_2O$, V_2O_5 and $Cu(NO_3)_2 \cdot 6H_2O$ were used to synthesize complex **1** ($CdCl_2 \cdot 2.5H_2O$ was used instead of $Cu(NO_3)_2 \cdot 6H_2O$ for complexes **2** and **3**). It should be noted that, the existence of vanadium in the reaction system seems to be important for the preparation of these complexes, because we failed to obtain the products by employing the same procedure without V_2O_5 although it has not been introduced into the target products as the heteroatom. The phenomenon seems strange but similar results have been reported previously though the mechanism relating to the role of vanadium ion is still ambiguous in the present stage [21,22].

3.2. Crystal structure

The single-crystal X-ray diffraction analysis reveals that complex **1** (Fig. 1) is composed of one $[H_2W_{12}O_{42}]^{10-}$ anion and two $Cu(H_2O)_2^{2+}$ cations which locate at the centers of the symmetry, eight sodium cations and some lattice water molecules. Considering the employed experimental condition, charge balance, temperature factor and the result of ICP, Na4 and Na8 are refined with 0.5 occupancies, respectively. The $Cu(H_2O)_2^{2+}$ cation exhibits typical chelated structure, in which Cu(II) ion is coordinated by two $[H_2W_{12}O_{42}]^{10-}$ anions. Obviously different from the complex **3**, the copper atom in complex **1** does not lie on the perpendicular bisector of two oxygen atoms of paradodecatungstate-B unit, showing Cu1–O bonding lengths of 1.919, 2.516 Å and Cu2–O of 1.925, 2.531 Å, respectively. It is normal for Cu-containing compounds having the similar coordination type. Due to the Jahn–Teller effect, there are usually weak Cu–O bonds with the distances of ca. 2.5 Å in the Cu-compounds as well as our present complex. The single-crystal structure analysis of complex **1** affirms the one-dimensional (1D) chain structure with the paradodecatungstate-B unit serving as a tetradentate ligand that coordinates to two $Cu(H_2O)_2^{2+}$ cations. This feature differs markedly from the reported 1D complex $[Cu(en)_2]_3[\{Cu(en)_2\}_2(H_2W_{12}O_{42})] \cdot 12H_2O$ [19], in which each paradodecatungstate-B cluster joins to four Cu atoms with the Cu–O distance of 2.493 and 2.538 Å and each Cu atom binds with POMs anion through single oxygen atom.

The crystal structure of **3**, presented in Fig. 2, can be described as a two-dimensional (2D) framework constructed from $Cd(H_2O)_2^{2+}$ cations and $[H_2W_{12}O_{42}]^{10-}$ clusters. Cd1 is six-coordinated and shows distorted octahedron geometry. The equatorial plane is defined by four oxygen atoms sourced from two neighboring paradodecatungstate-B units, and the axial positions are occupied by two water molecules with Cd–O distance of 2.422 Å. The Cd2 and Na4 atoms present a position disorder, possessing 0.30 and 0.70 occupations, respectively. Na5 and Na6 ions only occupy 0.35 and 0.5 of the sites based on the rationality of their atomic thermal displacement parameters, which is supported by the result of ICP. We have tried to solve the structure in lower symmetry space group to obtain the structure without disorder but it is not successful. In the structure of complex **3**, $[H_2W_{12}O_{42}]^{10-}$ cluster acts as an octadentate ligand that coordinates to four Cd^{2+} ions through the terminal oxygen atoms with the Cd–O bond lengths of 2.207 and 2.294 Å, respectively. Comparing with other transition metal bridging paradodecatungstate-B clusters [21], the present result exhibits the first example of 2D complex based on cadmium ions. Furthermore, the shape of the grid is like a gourd with the minimum distance of 3.188 Å and the maximum distance of 12.855 Å, respectively.

3.3. IR and TG analysis

In the IR spectrum (Fig. S1) of complex **1**, the vibration modes at 1630 and 1579 cm^{-1} can be attributed to the stretching modes of coordination and crystallization water molecules. The peaks at 943, 875, 835, 806, 710, 501 and 440 cm^{-1} can be clearly attributed to the vibration modes of $W{=}O_t$, $W{-}O_b{-}W$ and $W{-}O_c{-}W$ [23]. The IR spectra of complexes **2** and **3** exhibit the similar features to complex **1** (Fig. S2 and S3), which are consistent with the results of their crystal structures.

In the TG curve (Fig. S4) of complex **1**, the weight loss (10%) from room temperature to around 317 °C corresponds to the lattice water and weak coordinated water molecules (calc. 10.7%

Table 2
Selected bond lengths (Å) and angles (deg) for **1**, **2** and **3**

1		**2**		**3**	
Cu(1)–O(5)	1.921(8)	Cd1–O(21)	2.223(9)	Cd(1)–O(20)	2.201(8)
Cu(1)–O(43)	1.987(10)	Cd1–O(15)	2.300(9)	Cd(1)–O(21)	2.293(9)
Cu(1)–O(2)	2.520(14)	Cd1–O(22)	2.364(12)	Cd(1)–O(27)	2.425(11)
Cu(2)–O(42)	1.911(9)			Cd(2)–O(17)	2.261(8)
Cu(2)–O(44)	1.956(11)			Cd(2)–O(26)	2.409(14)
Cu(2)–O(22)	2.510(13)			Cd(2)–O(13)	2.414(9)
O(2)–Cu(1)–O(5)	91.0(4)	O(21)–Cd1–O(22)	88.5(4)	O(20)–Cd(1)–O(21)	93.9(3)
O(2)–Cu(1)–O(43)	95.0(4)	O(15)–Cd1–O(22)	92.9(4)	O(20)–Cd(1)–O(27)	86.4(3)
O(5)–Cu(1)–O(43)	91.7(4)	O(21)–Cd1–O(22)#1	91.5(4)	O(21)–Cd(1)–O(27)	93.1(3)
O(22)–Cu(2)–O(42)	91.1(4)	O(15)–Cd1–O(22)#1	87.1(4)	O(17)–Cd(2)–O(26)	85.9(5)
O(22)–Cu(2)–O(44)	86.1(4)	O(21)–Cd1–O(15)	91.3(3)	O(17)–Cd(2)–O(13)	91.0(3)
O(42)–Cu(2)–O(44)	89.9(4)	O(21)–Cd1–O(15)#1	88.7(3)	O(26)–Cd(2)–O(13)	79.7(5)

Symmetry code: #1 $-x+1$, $-y+2$, $-z+1$.

Fig. 1. Polyhedral representation of the one-dimensional chain of complex **1**. Color code: W atom, cyan and Cu atom, light green.

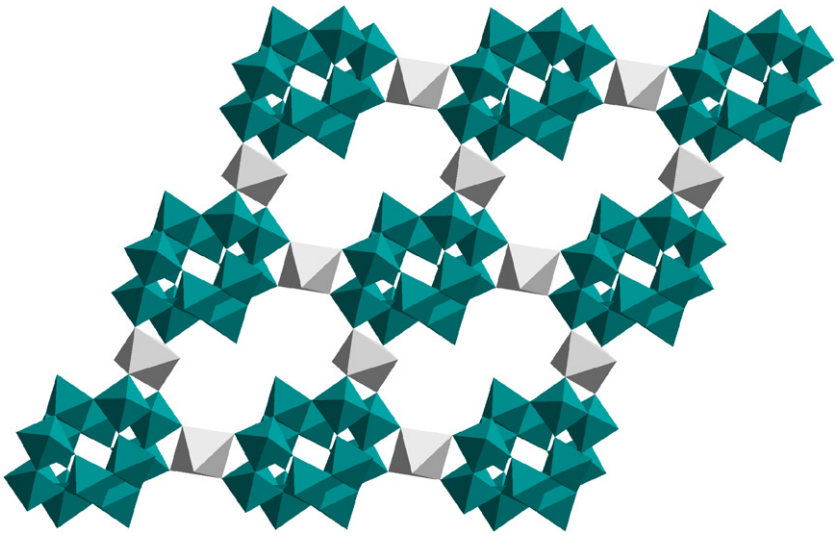

Fig. 2. Polyhedral representation of the two-dimensional network of complex **3**. Color code: W atom, cyan and Cd atom, light grey.

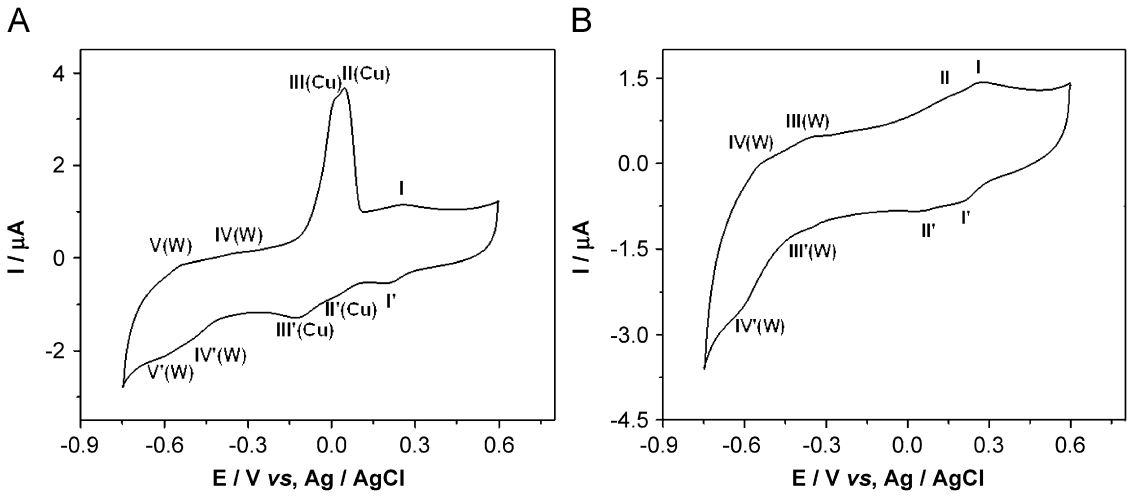

Fig. 3. Cyclic voltammograms of (A) 4.5×10^{-4} M of complex **1** and (B) 4.3×10^{-4} M of complex **3** in a buffer solution with pH 4.8 under the scan rate of 100 mV/s. The working electrode is glassy carbon and the reference electrode is Ag/AgCl.

for $H_{66}O_{74}Na_8CuW_{12}$). The number of lost water molecules in this stage is estimated 22. The second loss (2.4%) observed between 317 and 393 °C is in agreement with the losing assigned strong coordinated water molecules with sodium and copper (calc. 2.9%), and corresponds to six water molecules. Thus, the total number of water molecules from TGA is close to the molecules found from crystal structure. For complex **3**, TG curve (Fig. S5) shows that the weight loss (9%) from room temperature to around 293 °C is in agreement with the crystallized and weak water coordinated molecules with sodium atoms (calc. 10.2% for $H_{54}O_{68}Na_{7.4}Cd_{1.3}W_{12}$), corresponding to ca. 18 water molecules. The second weight loss (2%) observed between 293 and 386 °C is consistent with the loss (calc. 2.5%) of the strong coordinated water molecules with sodium and cadmium, corresponding to four water molecules.

3.4. Electrochemistry

Fig. 3A shows the typical cyclic voltammetric behavior of complex **1** under pH 4.8 buffer solution. Through using a GCE, five redox peaks appear in the potential range between 0.6 and −0.75 V and the mean peak potentials, $E_f=(E_{pa}+E_{pc})/2$, are 0.22 (I–I′), 0.017 (II–II′), −0.053 (III–III′), −0.44 (IV–IV′), and −0.58 V (V–V′) (vs. Ag/AgCl). The last two peaks IV–IV′ and V–V′ can be definitely ascribed to the redox of the $W^{VI/V}$ in the polyoxoanion framework as they can be also observed in other tungsten-containing POMs and they cannot be seen in blank buffer solution without complex **1** at the same pH. The second (II–II′) and third (III–III′) redox waves can be attributed to the redox of the Cu^{2+} ions corresponding to the two-step reduction of Cu^{2+} to Cu^{+} and Cu^{+} to Cu^{0}, as well as the two-step oxidation of Cu^{0} to Cu^{+} and Cu^{+} to Cu^{2+}. The similar results have been observed in other Cu-substituted POMs [24]. Unfortunately, we cannot assign the first redox wave (I–I′) surely, which may belong to the wave related to the redox of W. The following three points supported the speculation: (i) the same redox wave cannot be observed in blank buffer solution without complex **1**; (ii) there are no other active species in complex **1** other than W and Cu; and (iii) interestingly, the same redox wave clearly appears in the cyclic voltammogram (CV) of complex **3** under the same experimental condition.

The CV of complex **3** in pH 4.8 buffer solution is shown in Fig. 3B. It can be clearly seen that four redox peaks on a GCE were observed in the range of potential between 0.6 and −0.75 V and

the mean peak potentials are 0.23 (I–I′), 0.098 (II–II′), −0.35 (III–III′), and −0.57 V (IV–IV′) (vs. Ag/AgCl), respectively. The last two waves (III–III′) and (IV–IV′) are attributed to the redox processes of the $W^{VI/V}$ in complex **3**, as assigned for those of complex **1**. The first wave is similar to that at 0.22 V for (I–I′) of complex **1**. However, the range where the second wave II–II′ of complex **3** is located cannot be observed in CV for complex **1** that maybe was overlapped by redox peaks of Cu in complex **1**. The similar electrochemical behavior for the two complexes, except the redox for Cu in complex **1**, should be derived from the identical structure of the tungsten-oxo fragments. In addition, the CVs of complexes **1** and **3** vs. the scan rates under the same pH are investigated and shown in Fig. 4. By taking the oxidation peak I of complex **1** and the peak IV′ of complex **3** as the representatives, the peak currents of both complexes are linearly proportional to the square root of the scan rates, as shown in the inset of Fig. 4. This result indicates that the redox processes on electrode are diffusion-controlled for the two complexes.

3.5. Electrocatalysis

It is known that the nitrite existed in blood can oxidize hemoglobin to methemoglobin and make the former lose the capacity of carrying oxygen, causing hypoxia. Meanwhile, the high relative content of nitrate in drinking water can induce cancers. So, the detection for the existence and decomposition of nitrite and nitrate in biological system, acid rain and industrial waster, etc., become important [25]. In addition, nitrate is also usually used as the substrate for the examination of the electrocatalytic activity of Cu-, Fe- and Ni-containing compounds [24,26,27]. Because POMs could promote the electrochemical reduction of some molecules such as acidic radical anions, the two complexes are predicted to provide homogeneous electrocatalytic reduction for NO_2^-, which is not electroactive under the same experimental condition in blank buffer solution. Fig. 5 shows the CVs of the two complexes in NO_2^- solutions under various concentrations. For complex **1**, it can be seen clearly that the reduction currents increase with the addition of NO_2^- at the potential of −0.2 V where

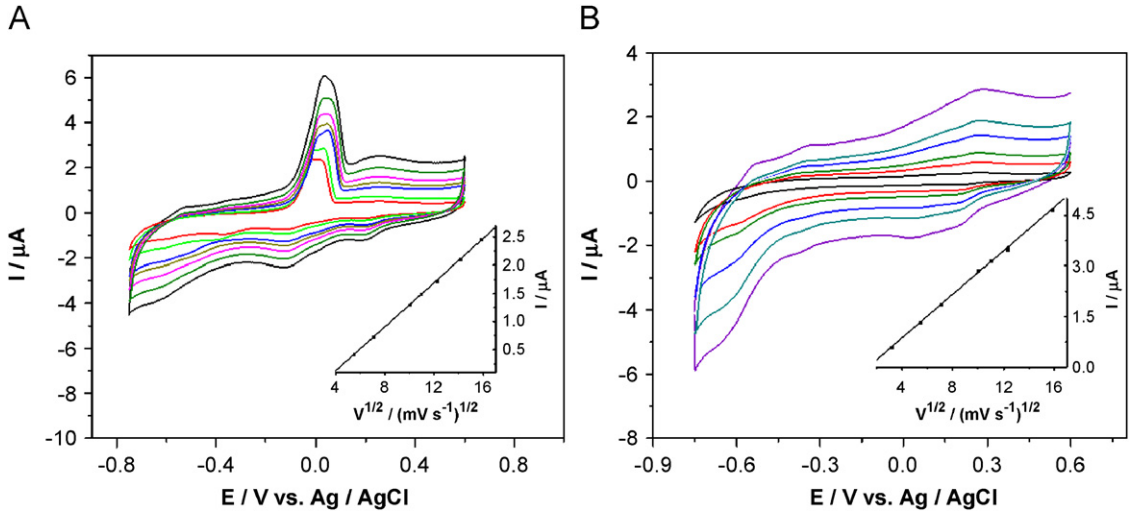

Fig. 4. Cyclic voltammograms of (A) 4.5×10^{-4} M complex **1** at different scan rates (from inner to outer: 30, 50, 100, 120, 150, 200 and 250 mV/s) and (B) 4.3×10^{-4} M complex **3** at different scan rates (from inner to outer: 10, 30, 50, 100, 120, 150, and 250 mV/s) in 0.5 M NaAc+HAc of buffer solution (pH 4.8). The insets show the relationship of the scan rate vs. the reduction peak currents of W.

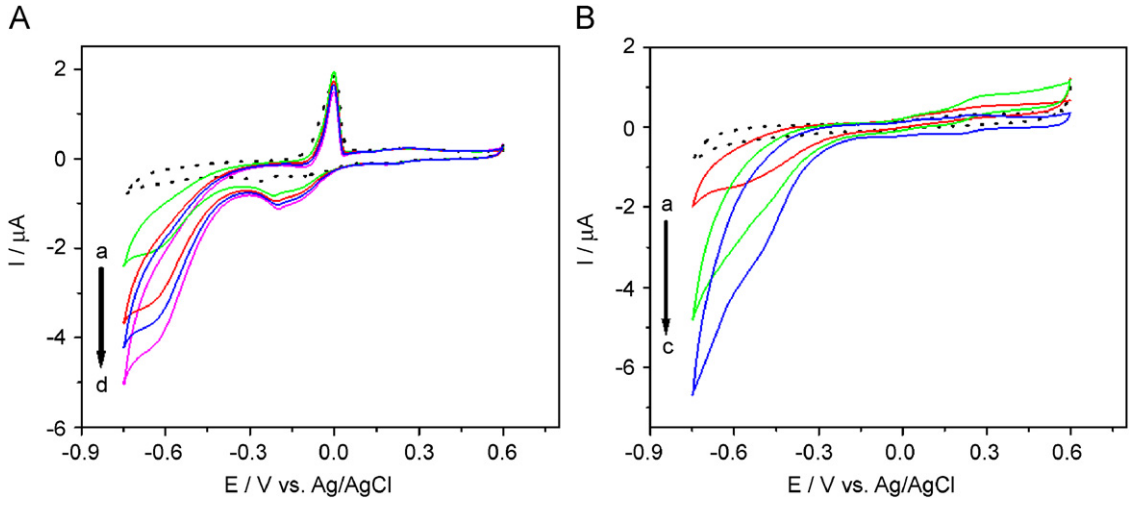

Fig. 5. Cyclic voltammograms of 4.5×10^{-4} M of complex **1** and 4.3×10^{-4} M of complex **3** in absence (dotted line) and presence (solid line) of the substrate at a scan rate: 10 mV/s. 0.5 M NaAc+HAc buffer solution (pH 4.8) containing NO_2^- at various concentrations: (A) for complex **1**, (a) 0.25, (b) 0.5, (c) 0.75, and (d) 1.25 mM (as arrow direction), and (B) for complex **3**, (a) 0.125, (b) 0.25, and (c) 1.25 mM (as arrow direction).

Cu(II) is reduced to Cu(0), and from which NO_2^- begins to be catalyzed. The increase of the reduction current should be sourced from the Cu(I) intermediate formed in the catalytic processes as mentioned in the literature [28]. At the potential of −0.35 V, W(VI) starts to be reduced to W(V), as shown in Fig. 5A. Similar results were also found in the CVs of other Cu(II)-substituted POMs [24,26]. Though the reduced species of W(VI) and Cu(II) are both electrocatalytic active for the reduction of NO_2^-, the reduced species of Cu(II) can catalyze NO_2^- at more positive potential than that of W(VI). So, it is evident that the Cu center plays an essential role in the catalytic reduction of NO_2^-. For complex **3**, as shown in Fig. 5B, from −0.35 V, the W-centered reduction currents begin to increase with increasing NO_2^- concentration and increase markedly at the potential of −0.6 V while its oxidation peak decreases. Therefore, we believe that the reduction of NO_2^- is more effectively electrocatalyzed by W center in complex **3**.

We also tested the electrocatalytic activities of the two complexes for the reduction of NO_3^-. Under the investigated potential region and experimental condition, no reduction of NO_3^- on the GCE surface could be observed in pH 4.8 blank buffer solutions. However, the electrocatalytic reduction of NO_3^- was detected in the presence of complex **1**. Complex **3** shows no electrocatalytic activity for the reduction of NO_3^-. The reason of the above-mentioned condition is perhaps that the reduced species of Cu(II) can catalyze NO_3^- to NO_2^- firstly, and the later can be further catalyzed by the reduced species of Cu(II) and W(VI). By the way, this explanation is oversimplified, and the veracious theory still needs to be investigated. As shown in Fig. 6, the reduction peak currents of the W(VI) and Cu(II) in the redox process increase dramatically with increasing NO_3^- concentration, indicating that the two reduced species of W and Cu possess electrocatalytic activity for the reduction of NO_3^-, starting from around −0.2 V. Similar results were also presented in other Cu (II)-substituted POMs [24,26].

3.6. Surface photovoltage properties

SPV measurement provides an effective tool for the characterization of semiconductor materials [29], as the combination of surface charge and illumination can determine surface voltage, oxide charge density, and mobile charge density oxide integrity and minority carrier diffusion length. Tungsten oxide bears pronounced photochromism properties upon bandgap photoexcitation, which makes it attractive and promising in many areas, especially in semiconductor materials [30]. Therefore, we employed surface photovoltage spectroscopy (SPS) and electric field-induced SPS (EFISPS) to study the materials properties of these complexes. Fig. 7A shows SPV property of complex **1** under zero and different positive bias. The photovoltaic response at about 330 nm corresponds to the band-to-band transition electrons for paradodecatungstate-B clusters, which has a little blue shift comparing to WO_3 powders [30]. With the increasing of positive bias, the peak position shifts slowly to the long wavelength, from 330 nm under zero bias towards 339 nm under 2 V of positive bias. On the other hand, the photovoltage value does not always increase with the larger positive bias given as n-type semiconductors. When 0.5 V of positive bias is set, the photovoltage reaches the highest value of 126.2 μV and then decreases to the values of 107.3 and 92.6 μV when 1.0 and 2.0 V of positive biases are applied, as shown in the inset of Fig. 7A. The reason forming the phenomenon is perhaps that the material surface is electricized when positive bias was provided. Fig. 7B shows that the SPS of complex **3** under zero and different positive biases. Similar to complex **1**, the photovoltaic response in the range from 325 to 339 nm also corresponds to the band-to-band transition electrons for paradodecatungstate-B clusters. But

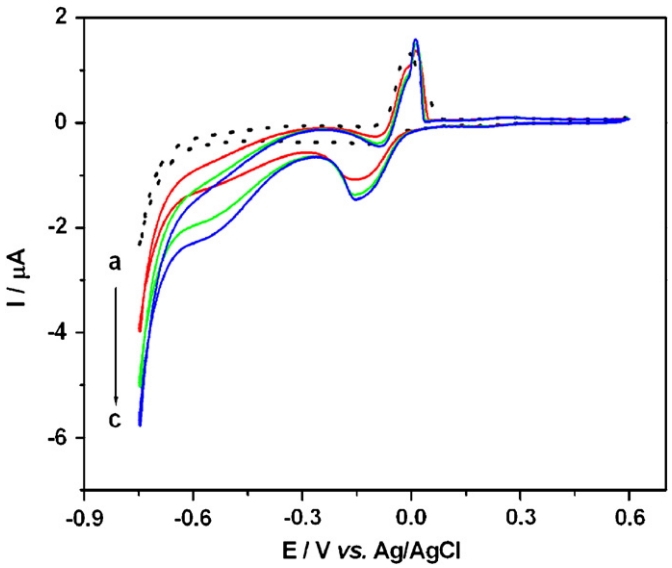

Fig. 6. Cyclic voltammograms of 6.0×10^{-4} M complex **1** in absence (dotted line) and presence (solid line) of the substrate at a scan rate of 2 mV/s. The buffer solution (0.5 M NaAc+HAc, pH 4.8) contains NO_3^- at various concentrations of (a) 0.25, (b) 0.5, and (c) 0.875 mM (as arrow direction).

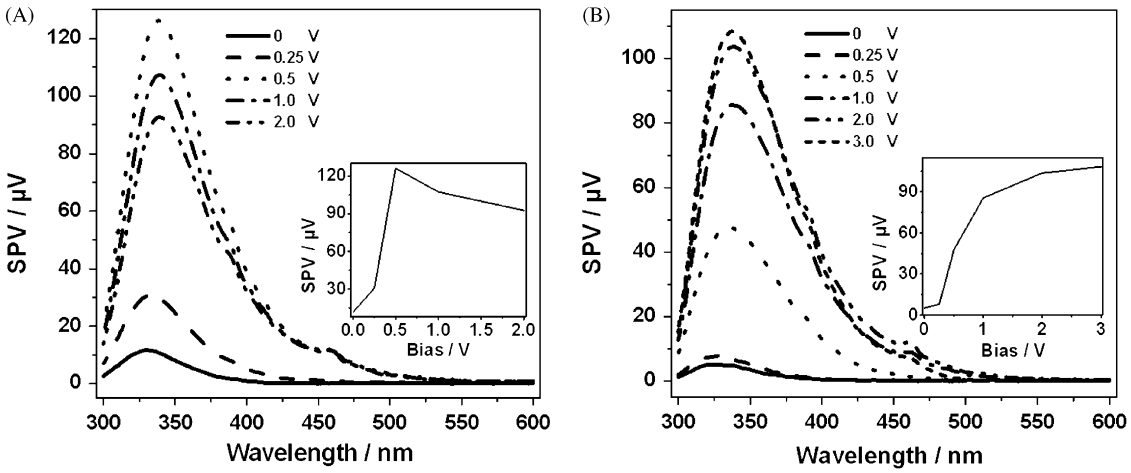

Fig. 7. Surface photovoltage spectra of (A) complex **1** and (B) complex **3** under different positive bias. The insets show the relationship of positive bias vs. peak values of SPV.

different from the complex **1**, the photovoltage values always increase when larger positive bias is given, as shown in the inset of Fig. 7B which shows complex **3** bearing a n-type semiconductor property [31]. Studies on the detailed and complete mechanism are currently underway.

4. Conclusion

In summary, we have demonstrated the synthesis and characterization of three complexes, $Na_8[Cu(H_2O)_2(H_2W_{12}O_{42})]\cdot 30H_2O$, $Na_8[Cd(H_2O)_2(H_2W_{12}O_{42})]\cdot 20H_2O$ and $Na_{7.4}[Cd_{1.3}(H_2O)_2(H_2W_{12}O_{42})]\cdot 24H_2O$. The structures of the first two complexes are 1D while the complex **3** possesses a 2D network structure, which enrich the structure types of copper and cadmium bridged paradodecatungstate-B clusters. The electrochemical behaviors of complexes **1** and **3** were studied by CV and the results exhibit successive W-centered reduction processes with similar peak potentials. Both complexes show the electrocatalytic activities towards the reduction of NO_2^-. In addition, complex **1** undergoes the redox reactions originating from the Cu center, resulting in the electrocatalytic activity for the reduction of NO_3^- while complex **3** does not hold. The behaviors of SPS and EFISPS with supplied positive bias show that the SPV behavior of complex **1** is complicated while complex **3** bears the property of n-type semiconductor.

Supplementary data

CSD numbers, 419058, 419057 and 419056 contain the supplementary crystallographic data for **1**, **2** and **3**, respectively. These data can be obtained from the Fachinformationszentrum Karlsruhe, D-76344 Eggenstein-Leopoldshafen, Germany (E-mail: Crysdata@fiz-karlstruhe.de). IR spectra and TG curves for **1** and **3** are presented in the Supporting Information.

Acknowledgments

The authors acknowledge the financial support from National Basic Research Program (2007CB808003), National Natural Science Foundation of China (20703019, 20731160002), PCSIRT of Ministry of Education of China (IRT0422), and 111 Project (B06009) for the supporting of the collaboration with Prof. Loodsrecht at University of Groningen.

Appendix A. Supplementary material

Supplementary data associated with this article can be found in the online version at doi:10.1016/j.jssc.2008.09.009.

References

[1] (a) M.T. Pope, Heteropoly and Isopoly Oxometalates, Springer, Berlin, 1983;
(b) M.T. Pope, A. Müller, Polyoxometalate Chemistry from Topology via Self-Assembly to Application, Kluwer Academic Publishers, Dordrecht, 2001;
(c) C.L. Hill, Chem. Rev. 98 (1998) 1–2.
[2] (a) A. Müller, S.K. Das, H. Bögge, C. Beugholt, M. Schmidtmann, Chem. Commun. (1999) 1035–1036;
(b) C.P. Pradeep, D.L. Long, P. Kögerler, L. Cronin, Chem. Commun. (2007) 4254–4256;
(c) U. Kortz, F. Hussain, M. Reicke, Angew. Chem. Int. Ed. 44 (2005) 3773–3777;
(d) S.S. Mal, U. Kortz, Angew. Chem. Int. Ed. 44 (2005) 3777–3780.
[3] (a) P.J. Hagrman, D. Hagrman, J. Zubieta, Angew. Chem. Int. Ed. 38 (1999) 2638–2684;
(b) M.I. Khan, E. Yohammes, D. Powell, Chem. Commun. (1999) 23–24;
(c) B.B. Yan, Y. Xu, X.H. Bu, N.K. Goh, L.S. Chia, G.D. Stucky, J. Chem. Soc. Dalton Trans. (2001) 2009–2014;
(d) Y. Lu, Y. Xu, Y.G. Li, E.B. Wang, X.X. Xu, Y. Ma, Inorg. Chem. 45 (2006) 2055–2060.
[4] (a) C.J. Warren, D.J. Rose, R.C. Haushalter, J. Zubieta, Inorg. Chem. 37 (1998) 1140–1141;
(b) A. Müller, M. Koop, P. Schiffels, H. Bögge, Chem. Commun. (1997) 1715–1716.
[5] (a) E. Burkholder, S. Wright, V. Golub, C.J. O'Connor, J. Zubieta, Inorg. Chem. 42 (2003) 7460–7471;
(b) J.Q. Sha, J. Peng, H.S. Liu, J. Chen, B.X. Dong, A.X. Tian, Z.M. Su, Eur. J. Inorg. Chem. (2007) 1268–1274;
(c) H.Y. An, D.R. Xiao, E.B. Wang, Y.G. Li, Z.M. Su, L. Xu, Angew. Chem. Int. Ed. 45 (2006) 904–908;
(d) Y.P. Ren, X.J. Kong, X.Y. Hu, M. Sun, L.S. Long, Inorg. Chem. 45 (2006) 4016–4024;
(e) J.X. Chen, T.Y. Lan, Y.B. Huang, C.X. Wei, Z.S. Li, J. Solid State Chem. 179 (2006) 1904–1911.
[6] Z.M. Zhang, J. Liu, E.B. Wang, C. Qin, Y.G. Li, Y.F. Qi, X.L. Wang, Dalton Trans. (2008) 463–468.
[7] L.J. Zhang, Y.G. Wei, C.C. Wang, H.Y. Guo, P. Wang, J. Solid State Chem. 177 (2004) 3433–3438.
[8] D. Hagrman, P.J. Zapf, J. Zubieta, Chem. Commun. (1998) 1283–1284.
[9] J. Tao, X.M. Zhang, M.L. Tong, X.M. Chen, J. Chem. Soc. Dalton Trans. (2001) 770–771.
[10] B.Z. Lin, S.X. Liu, Chem. Commun. (2002) 2126–2127.
[11] R. Allmann, Acta Crystallogr. B 27 (1970) 1393–1404.
[12] M.T. Averbuch-Pouchot, L. Tordjman, A. Durif, J.C. Guitel, Acta Crystallogr. B 35 (1979) 1675–1677.
[13] H. Naruke, N. Fukuda, T. Yamase, Acta Crystallogr. C 56 (2000) 177–178.
[14] G.J. Gainsford, N. Robinson, J.L. Tallon, Acta Crystallogr. E 58 (2002) m521–m523.
[15] G.J. Gainsford, S.V. Chong, B. Ingham, J.L. Tallon, Acta Crystallogr. E 58 (2002) i93–i94.
[16] X.T. Zhang, D.Q. Wang, J.M. Dou, S.S. Yan, X.X. Yao, J.Z. Jiang, Inorg. Chem. 45 (2006) 10629–10635.
[17] C. Giménez-Saiz, J.R. Galán-Mascarós, S. Triki, E. Coronado, L. Ouahab, Inorg. Chem. 34 (1995) 524–526.
[18] W.B. Yang, C.Z. Lu, X.L. Lin, H.H. Zhang, Z. Anorg. Allg. Chem. (629) (2003) 2046–2052.
[19] B.Z. Lin, Y.M. Chen, P.D. Liu, Dalton Trans. (2003) 2474–2475.
[20] L. Lisnard, A. Dolbecq, P. Mialane, J. Marrot, F. Sécheresse, Inorg. Chem. Acta 357 (2004) 845–852.
[21] C.Y. Sun, S.X. Liu, L.H. Xie, C.L. Wang, B. Gao, C.D. Zhang, Z.M. Su, J. Solid State Chem. 179 (2006) 2093–2100.
[22] H.T. Evans Jr., O.W. Rollins, Acta Crystallogr. B 32 (1976) 1565–1567.
[23] Z.M. Zhang, Y.F. Qi, C. Qin, Y.G. Li, E.B. Wang, X.L. Wang, Z.M. Su, L. Xu, Inorg. Chem. 46 (2007) 8162–8169.
[24] (a) B. Keita, I.M. Mbomekalle, L. Nadjo, Electrochem. Commun. 5 (2003) 830–837;
(b) B. Keita, E. Abdeljalil, L. Nadjo, R. Contant, R. Belghiche, Langmuir 22 (2006) 10416–10425;
(c) S. Nellutla, J. Van Tol, N.S. Dalal, L.H. Bi, U. Kortz, B. Keita, L. Nadjo, G.A. Khitrov, A.G. Marshall, Inorg. Chem. 44 (2005) 9795–9806.
[25] S.Y. Zhai, S.Y. Gong, J.G. Jiang, S.J. Dong, J.H. Li, Anal. Chim. Acta 486 (2003) 85–92.
[26] (a) B. Keita, I.M. Mbomekalle, L. Nadjo, R. Contant, Electrochem. Commun. 3 (2001) 267–273;
(b) D. Jabbour, B. Keita, L. Nadjo, U. Kortz, S.S. Mal, Electrochem. Commun. 7 (2005) 841–847.
[27] (a) L.H. Bi, U. Kortz, S. Nellutla, A.C. Stowe, J. Van Tol, N.S. Dalal, B. Keita, L. Nadjo, Inorg. Chem. 44 (2005) 896–903;
(b) D. Jabbour, B. Keita, I.M. Mbomekalle, L. Nadjo, U. Kortz, Eur. J. Inorg. Chem. (2004) 2036–2044.
[28] J.E. Toth, F.C. Anson, J. Am. Chem. Soc. 111 (1989) 2444–2451.
[29] L. Kronik, Y. Shapira, Surf. Sci. Rep. 37 (1999) 1–206.
[30] T. He, J.N. Yao, J. Mater. Chem. 17 (2007) 4547–4557.
[31] R.G. Xie, J.Q. Zhuang, L.L. Wang, W.S. Yang, D.J. Wang, T.J. Li, J.N. Yao, Chem. J. Chin. Univ. 24 (2003) 2086–2088.